

Constraining the Mass Distribution of Cluster Galaxies by Weak Lensing

Bernhard Geiger

Max-Planck-Institut für Astrophysik, Karl-Schwarzschild-Straße 1, Postfach 1523,
D-85740 Garching bei München, Germany

Abstract. Analysing the weak lensing distortions of the images of faint background galaxies provides a means to constrain the mass distribution of cluster galaxies and potentially to test the extent of their dark matter halos as a function of the density of the environment. Here I describe simulations of observational data and present a maximum likelihood method to infer the average properties of an ensemble of cluster galaxies.

1 Introduction

Measurements of the rotation curves of spiral galaxies indicate that they are embedded in massive dark matter halos. The deflection of light rays through the gravitational action of mass concentrations, usually called gravitational lensing, provides a way to obtain information about the mass distribution of galaxies at radial distances from their centre where there are no more luminous test particles to probe the gravitational potential. The light deflection causes small distortions of the images of faint background galaxies. Recent statistical analyses (Brainerd et al. 1996, Griffiths et al. 1996) of these weak distortion effects suggest that the dark galaxy halos are indeed rather extended, as some popular theories of structure formation predict them to be. During the formation of galaxy clusters the extended halos of galaxies may be stripped off due to tidal forces of the cluster potential or during encounters with other galaxies. Ultimately the individual galaxy halos should merge and form a global cluster halo. In this contribution I discuss how this merging picture could be tested observationally by exploiting the weak lensing effects.

The distortions of the images of background galaxies produced by massive galaxy clusters are strong enough to allow a parameter-free reconstruction of the clusters' surface mass density, and several algorithms have been developed for this purpose (e.g. Kaiser and Squires 1993, Seitz and Schneider 1995, 1996). The smoothing length which has to be implemented in these techniques, however, is larger than galaxy scales, i.e., the amount of information available does not suffice to reconstruct cluster galaxies individually. Therefore, one has to superpose the effects of a large number of galaxies statistically in order to infer the average properties of an ensemble of galaxies.

Section 2 presents simulations of a galaxy cluster which are sufficiently realistic for the purposes of this work, and demonstrates how individual galaxies modify the distortion pattern of a smooth cluster mass distribution. Section 3

discusses a maximum likelihood method for constraining the mass distribution of cluster galaxies, and Sect. 4 presents results of the simulations. Finally, in Sect. 5 some suggestions for refining the simulations are mentioned, and observational prospects are discussed. A closely related work was recently published by Natarajan and Kneib (1997); in contrast to their maximum likelihood method, the mass profile of the cluster is not assumed to be known but is reconstructed from image distortions as mentioned above.

2 Simulations

2.1 Cluster and Cluster Galaxies

A galaxy cluster with a total mass of about $10^{15}h^{-1}M_{\odot}$ located at a redshift of $z_d = 0.16$ was selected from numerical N-body simulations (Bartelmann et al. 1995). Within this paper a quadratic field of view with side length $10'$ is considered, which roughly corresponds to a physical size of $1h^{-1}$ Mpc at the cluster redshift. In order to populate the dark matter distribution of this cluster with galaxies the following requirements were specified:

1. The total mass-to-light ratio of the cluster was chosen to be $300hM_{\odot}/L_{\odot}$.
2. Galaxy luminosities L were drawn from a Schechter function with canonical parameters (and a cutoff at $0.1L_{\star}$).
3. Galaxy positions were randomly drawn from those of the N-body particles.

This procedure resulted in a rich cluster of 359 galaxies, 40 of which are brighter than L_{\star} . For the mass distribution of the cluster galaxies, a simple truncated isothermal sphere (Brainerd et al. 1996) was used. The surface mass density Σ as a function of the projected radius ξ is given by

$$\Sigma(\xi) = \frac{\sigma^2}{2G\xi} \left(1 - \frac{\xi}{\sqrt{s^2 + \xi^2}} \right), \quad (1)$$

where the two parameters, velocity dispersion σ and cutoff radius s , were chosen as functions of the luminosity according to the following scaling relations:

$$\sigma = \sigma_{\star} \left(\frac{L}{L_{\star}} \right)^{1/\eta} \quad \text{and} \quad s = s_{\star} \left(\frac{L}{L_{\star}} \right)^{\nu}. \quad (2)$$

For the first of these relations, which is motivated by the observed Tully-Fisher and Faber-Jackson relations, a value of $\eta = 4$ was used for the scaling index and the velocity dispersion σ_{\star} of an L_{\star} -galaxy was fixed at 200 km/s. For simplicity, no distinction between spiral and elliptical galaxies was made. The scaling relation for the cutoff radius is more conjectural, and choosing $\nu = 0.5$ yields a mass-to-light ratio for the galaxies which is independent of luminosity. To test the method, two models were used for the cutoff radius. Choosing $s_{\star} = 3.4h^{-1}$ kpc gives a total L_{\star} -galaxy mass of $M_{\star} = 10^{11}h^{-1}M_{\odot}$, whereas an extended halo of $s_{\star} = 34h^{-1}$ kpc results in $M_{\star} = 10^{12}h^{-1}M_{\odot}$. These galaxy mass models were added to the global cluster mass distribution, which was scaled such that the total mass of the system remains constant (see Fig. 1 left).

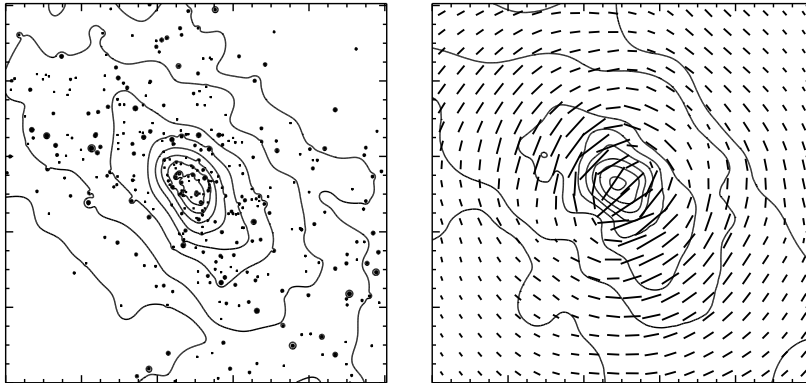


Fig. 1. Left: The mass distribution of the cluster including the cluster galaxies with $s_* = 34h^{-1}$ kpc. Right: The distortion pattern determined from the ellipticities of background galaxy images overlaid with the reconstructed cluster mass distribution. The field of view is $10'$ and the contours are $\kappa = 0.05, 0.1, 0.2, 0.3, 0.4, 0.5, 0.6,$ and 0.7 .

2.2 Distortion Effects and Background Galaxies

The lensing properties of the galaxy cluster are specified by the dimensionless surface mass density κ and the (complex) shear γ which are second derivatives of a common two-dimensional scalar potential. However, image distortions are only sensitive to the combined quantity $g = \gamma/(1 - \kappa)$. Figure 2 shows a map of $|g|$, which is a measure of the strength of the distortion effects on the images of background galaxies. In general, these distortions tend to be aligned tangentially towards the centre of mass concentrations. The figure illustrates the perturbing effects of the individual cluster galaxies. At their positions in a radial direction towards and away from the cluster centre the strength of the distortion is locally increased because the effects of the global cluster mass distribution and the cluster galaxy then act in the same direction. But in the direction tangential to the cluster centre the orientation of the galaxy contribution to the shear is perpendicular to the cluster's shear direction, and therefore these effects cancel out which leads to a reduction in the strength of the distortion effects.

Unfortunately Nature does not provide us with a continuous map of the lensing properties, but only with very noisy estimates of the parameter g at the discrete positions of background galaxy images. For these simulations, a random population of background galaxies was generated with a number density of $40/\text{arcmin}^2$, including a realistic intrinsic ellipticity distribution and a reasonable redshift distribution. Figure 1 (right) shows the gridded distortion pattern calculated from the ‘observed’ ellipticities of the background galaxy images by employing a suitable averaging procedure. This figure also displays the reconstruction of the mass distribution using a finite-field non-linear inversion method (Seitz and Schneider 1996).

Fig. 2. The modulus $|g|$ of the reduced shear. This quantity is a measure for the strength of the distortion effects.

3 Method

In order to constrain the mass distribution of cluster galaxies a maximum likelihood method was developed which follows in part the prescription of Schneider and Rix (1997) for weak lensing by field galaxies. The image distortions are a consequence of the interplay between the effects of a global cluster potential and the perturbations due to individual galaxies. In addition to specifying a parametrized mass model for the galaxies it is, therefore, important to have an accurate description of the cluster mass distribution which is provided by the reconstruction mentioned above. As a model for the galaxy mass distribution I again used the truncated isothermal sphere (1). Of course, this model is appro-

appropriate for the simulated data used here, whereas one could argue that realistic galaxy halos in clusters might rather be flattened or completely irregular. However, this analysis is aimed at determining the average properties of an ensemble of galaxies which might still be reasonably described by a simple model with a characteristic scale and normalization as parameters. In order to add the information from galaxies with different luminosities, the scaling relations (2) were applied. Adding the mass models for each of the cluster galaxies to the cluster reconstruction then yields a model for the total mass distribution of the system as a function of the velocity dispersion σ_* and the cutoff radius s_* of an L_* -galaxy. A complication which has to be taken into account when performing this procedure is the following. If the individual galaxies do have extended halos, the mass in galaxies constitutes a significant fraction of the total cluster mass ($\approx 30\%$ for the model with $s_* = 34h^{-1}$ kpc). The cluster reconstruction is sensitive to the total mass and therefore it already includes the masses of the galaxies. This means that the additional mass added by the galaxy models has to be compensated in some way. This was done by simply scaling down the reconstruction appropriately or by subtracting surplus mass locally on scales of roughly $1'$ at the position of cluster galaxies. The merits and limitations of this (*ad hoc*) procedure will be discussed in Sect. 4.

The total mass model constructed in this way determines the values for the lensing parameters κ and γ at the position of each background galaxy image. The strength of the lensing effect also depends on the distance of the sources, and in the following the symbols κ_∞ and γ_∞ are used to indicate the reference to (hypothetical) sources located at infinite redshift. The probability density $p_\epsilon(\epsilon | \kappa_\infty, \gamma_\infty)$ for observing the (complex) image ellipticity ϵ if the source is lensed by the specified mass model is given by

$$p_\epsilon(\epsilon | \kappa_\infty, \gamma_\infty) = \int_0^\infty dz p_z(z) p_{\epsilon_s}(\epsilon_s(\epsilon | \kappa_\infty, \gamma_\infty, z)) \left| \frac{d^2 \epsilon_s}{d^2 \epsilon} \right| (\epsilon | \kappa_\infty, \gamma_\infty, z). \quad (3)$$

To calculate this probability, it is necessary to know the intrinsic ellipticity distribution $p_{\epsilon_s}(\epsilon_s)$ of the sources, which can be determined from ‘empty’ fields, and an estimate for the redshift distribution $p_z(z)$. In addition, non-linear properties of the lens mapping have to be taken into account, and the last term under the integral is the Jacobian determinant for the transformation of image ellipticities ϵ to source ellipticities ϵ_s . The likelihood function \mathcal{L} is defined as the product of the probability densities of the actually measured ellipticities ϵ_i of all the background galaxy images:

$$\mathcal{L} = \prod_i p(\epsilon_i). \quad (4)$$

The best-fit galaxy mass distribution and confidence regions can then be found by maximizing this likelihood function with respect to the parameters of the model. The logarithm of the likelihood function is denoted as $l = \ln \mathcal{L}$, and in the next section contour plots of $\Delta l = l - l_{\text{Max}}$ as a function of the model parameters will be presented.

4 Results

4.1 Velocity Dispersion and Cutoff Radius

Figure 3 (left) shows the result of the maximum likelihood analysis for the input galaxy model with a small cutoff radius of $s_\star = 3.4h^{-1}$ kpc. For this plot a total number of 3978 background galaxies from the entire field of view were included in the calculation of the likelihood function. The confidence region closely follows the dashed line of models with equal mass within a (projected) radius of $6h^{-1}$ kpc, which means that this is the quantity which can be determined best with this lensing method. However, the velocity dispersion and the cutoff radius individually cannot be well determined from the data. This result is not surprising because all background galaxy images which are located closer to cluster galaxies than roughly this distance of $6h^{-1}$ kpc have been excluded from the analysis as they will be outshone by the light of the cluster galaxy, and so there is no information available about the distribution of the mass inside this radius. But still it is possible to obtain tighter limits on the cutoff radius by including *a priori* knowledge on the velocity dispersion σ_\star . If we believe that the measured velocity dispersions of elliptical galaxies or the rotational velocities of spirals (divided by a factor of $\sqrt{2}$) represent the same quantity as the parameter σ of the dark matter halo model, we can include this knowledge into the likelihood function. Figure 3 (right) demonstrates the results after adding the prior information of $\sigma_\star = 200 \pm 20$ km/s. In this case very interesting limits on s_\star can be achieved.

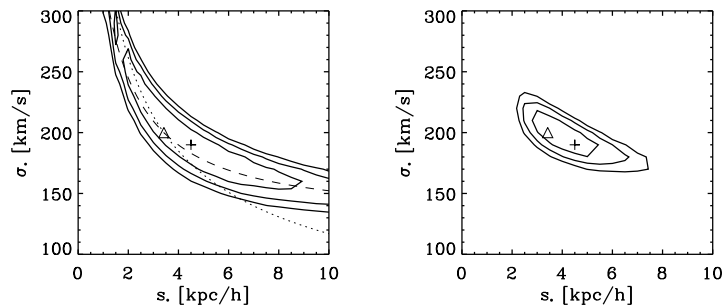


Fig. 3. The logarithm of the likelihood as a function of the velocity dispersion σ_\star and the cutoff radius s_\star . The contours are $\Delta l = -1, -2, -3$. The triangles denote the input values and the crosses mark the maximum of the likelihood function. **Left:** Only including information provided by the lensing analysis. The dotted line connects models with equal total mass and along the dashed line the mass within a projected radius of $6h^{-1}$ kpc is constant. **Right:** The likelihood contours after adding the prior information of $\sigma_\star = 200 \pm 20$ km/s.

In Fig. 4 the same data is divided into two independent subsets according to the location of the background galaxy images. The left panel shows the contours of the logarithm of the likelihood function (without prior information) using all images (3714) whose distances from the cluster centre exceed $1'.5$ and in the right panel all images (264) within this limit were used. The number of cluster galaxies which are located in these areas are 265 and 94, respectively. The figure shows that the far fewer images in the centre provide almost the same amount of information as the numerous images in the outskirts of the cluster. The reasons for this are the higher cluster galaxy density in the centre and the significant enhancement of the distortion effects of individual cluster galaxies due to the underlying cluster mass distribution. Hence it is feasible to test a possible dependence of the extent of galaxy dark matter halos on the density of the environment by binning the data appropriately.

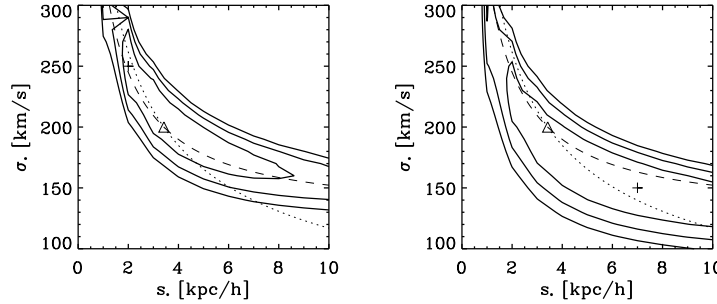


Fig. 4. The same as Fig. 3 (left) but after dividing the data set into background galaxies with a distance from the cluster centre larger than $1'.5$ (left) and less than $1'.5$ (right).

Figure 5 displays the results for the same realization of background galaxies as above – but here a large input value was used for the cutoff radius of the cluster galaxies ($s_* = 34h^{-1}$ kpc). The left plot, calculated from images in the outer region of the cluster, shows that in this case the velocity dispersion can be reasonably well determined, whereas the lensing effects are less sensitive to the radial extent of the mass distribution. Nevertheless a robust lower limit of about $15h^{-1}$ kpc can be set for the cutoff radius, and so this model can be distinguished with high significance from the low- s_* model used above. Figure 5 (right) reveals the problems of the method when it is applied to the images located in the cluster centre. The input values cannot be reproduced by the likelihood analysis in this case. The reason for this is the ambiguity introduced by the mass correction procedure referred to in Sect. 3. This problem does not show up for the input model with small cutoff radius because then the mass in galaxies only amounts to a few percent of the total mass, and the mass correction is not important. In the

outer regions of the cluster, the problem is less severe, because the requirements for the accuracy of the cluster mass reconstruction are less stringent in the weak lensing regime when the surface mass density is low and so the method works there even when the galaxies are massive (Fig. 5 left). In the non-linear lensing regime of the cluster centre, however, an accurate description of the cluster mass distribution is essential to obtain reliable results.

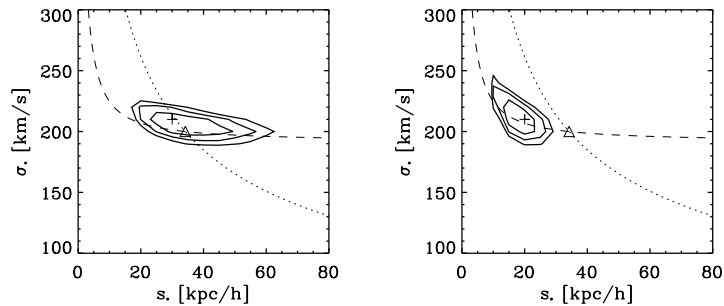


Fig. 5. The results of the likelihood analysis for a cluster galaxy input model with an extended dark matter halo. Note the change of scale on the x-axis compared to the previous figures. The binning of the data into information coming from images in the outer regions of the cluster (**left**) and the cluster centre (**right**) is the same as in Fig. 4.

In order to solve the problem becoming apparent in Fig. 5 (right) one might envisage employing a maximum likelihood reconstruction of the cluster mass distribution in the fashion of Bartelmann et al. (1996). In such a method the presence of cluster galaxies could be taken into account explicitly during the reconstruction process. For each set of parameters of the galaxy mass model, one can then determine the best representation of the underlying cluster mass distribution. Therefore, this approach would also be more satisfactory in a full maximum likelihood sense. Finally, I would like to remark that making the distinction between dark matter associated to galaxies or belonging to a global cluster mass distribution becomes somewhat artificial in the very centre of galaxy clusters when the physical distances between the galaxies become very small, and clearly the giant cD-galaxies residing in the centre of many clusters cannot be treated with the same formalism as ordinary cluster galaxies.

4.2 Scaling Parameters

In addition to σ_* and s_* , a full description of the model for the galaxy mass distribution also requires to specify the power indices of the scaling relations (2). In the previous subsection the same values ($\eta = 4$, $\nu = 0.5$) that had been

used to generate the data were taken for the likelihood analysis, but giving up that restriction and varying the scaling parameters within reasonable ranges does not affect the general conclusions drawn there.

Here the prospects for determining these scaling indices from the lensing analysis are briefly mentioned. For generating the data the galaxy model with the small cutoff radius has been adopted. Figure 6 depicts contour plots for the logarithm of the likelihood as a function of $1/\eta$ and σ_* (left) and ν and σ_* (right) including the background images from the whole field of view. Each time the two remaining parameters were fixed at the input values. The plots show that the constraints on the scaling indices are not particularly tight. In order to improve them it would be necessary to add the information from several galaxy clusters.

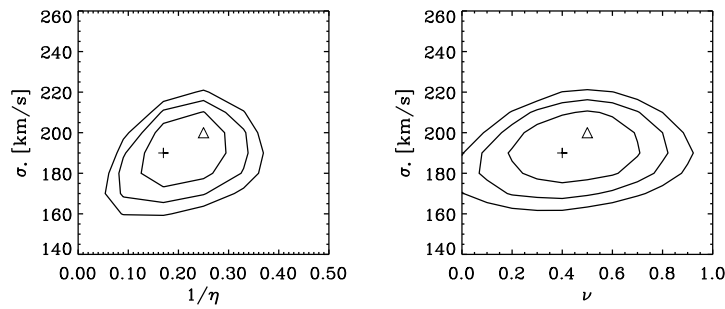


Fig. 6. The dependence of the likelihood function on the scaling indices η and ν . Again, the contours are $\Delta l = -1, -2, -3$, the triangles denote the input values and the crosses mark the maximum of the likelihood function.

5 Prospects

5.1 Simulations

There are several ways in which the simulations presented here could be refined. A distinction should be made between spiral and elliptical cluster galaxies because they require different normalizations for the velocity dispersion. An obvious thing to do is to explicitly include a dependence of the cutoff radius as a function of the (three-dimensional) density of the environment. One can then develop strategies to quantify this dependence and to assess the uncertainties introduced by projection effects. For this study it was assumed that cluster galaxies and background galaxies can be unambiguously distinguished by means of some colour criterion. The importance of this assumption can be tested by deliberately misinterpreting faint cluster galaxies as background galaxies. First

investigations in this direction indicate that this is a minor problem, because the main part of the signal is contributed by the more massive cluster galaxies.

5.2 Observations

Weak lensing is a challenging project from the observational point of view, because it necessitates measuring accurate image ellipticities for a large number of faint galaxies. To achieve the galaxy number density of $40/\text{arcmin}^2$ used in this simulations requires deep observations with a magnitude limit of about 25. The unique image quality of the (refurbished) Hubble Space Telescope allows to determine image ellipticities with a high accuracy, and in this respect it is the ideal instrument for weak lensing purposes. Its drawback, on the other hand, is the rather small field of view of its ‘wide field’ camera, and so time consuming mosaics of several images are required in order to completely cover a cluster which is located at a reasonable redshift. However, it has been shown in recent years that ground-based observations can be used for weak lensing studies as well, provided that they were taken in good seeing and with telescopes and instruments whose imaging properties are sufficiently well understood. Several observations – from space as well as from the ground – which are suitable for carrying out the kind of analysis described in this contribution are already available, and clearly this will be a rewarding project for the VLT-era.

Acknowledgments. I thank Matthias Bartelmann for making the N-body cluster simulation available, Peter Schneider and Stella Seitz for discussions and for providing the reconstruction algorithm, and Matthias and Peter for comments on the manuscript. This work was supported in part by the Sonderforschungsbereich 375-95 der Deutschen Forschungsgemeinschaft.

References

- Bartelmann, M., Narayan, R., Seitz, S., Schneider, P. (1996), *ApJ*, 464, L115
 Bartelmann, M., Steinmetz, M., Weiss, A. (1995), *A&A*, 297, 1
 Brainerd, T.G., Blandford, R.D., Smail, I. (1996), *ApJ*, 466, 623
 Griffiths, R.E., Casertano, S., Im, M., Ratnatunga, K.U. (1996), *MNRAS*, 282, 1159
 Kaiser, N., Squires, G. (1993), *ApJ*, 404, 441
 Natarajan, P., Kneib, J.-P. (1997), *MNRAS*, in press
 Schneider, P., Rix, H.-W. (1997), *ApJ*, 474, 25
 Seitz, C., Schneider, P. (1995), *A&A*, 297, 287
 Seitz, S., Schneider, P. (1996), *A&A*, 305, 383

This figure "fig_distortion.jpeg" is available in "jpeg" format from:

<http://arxiv.org/ps/astro-ph/9701070v2>